Supporting Information

Exchange-spring mechanism and Griffiths-like phase in room-temperature magnetoelectric Ni-$BaTiO_3$ composites

Ramany Revathy[1], Nandakumar Kalarikkal[2], Manoj Raama Varma[1, 3, *], Kuzhichalil Peethambharan Surendran[1, 3, *]

[1]*Materials Science and Technology Division, CSIR- National Institute for Interdisciplinary Science and Technology Division (NIIST), Research Centre, University of Kerala, Industrial Estate P.O., Thiruvananthapuram -695019, India*

[2]*International & Inter University Centre for Nanoscience and Nanotechnology, Mahatma Gandhi University, Kottayam, Kerala-686560, India*

[3]*Academy of Scientific and Innovative Research, Ghaziabad, Uttar Pradesh- 201002, India*

E-mail: manoj@niist.res.in, kpsurendran@niist.res.in

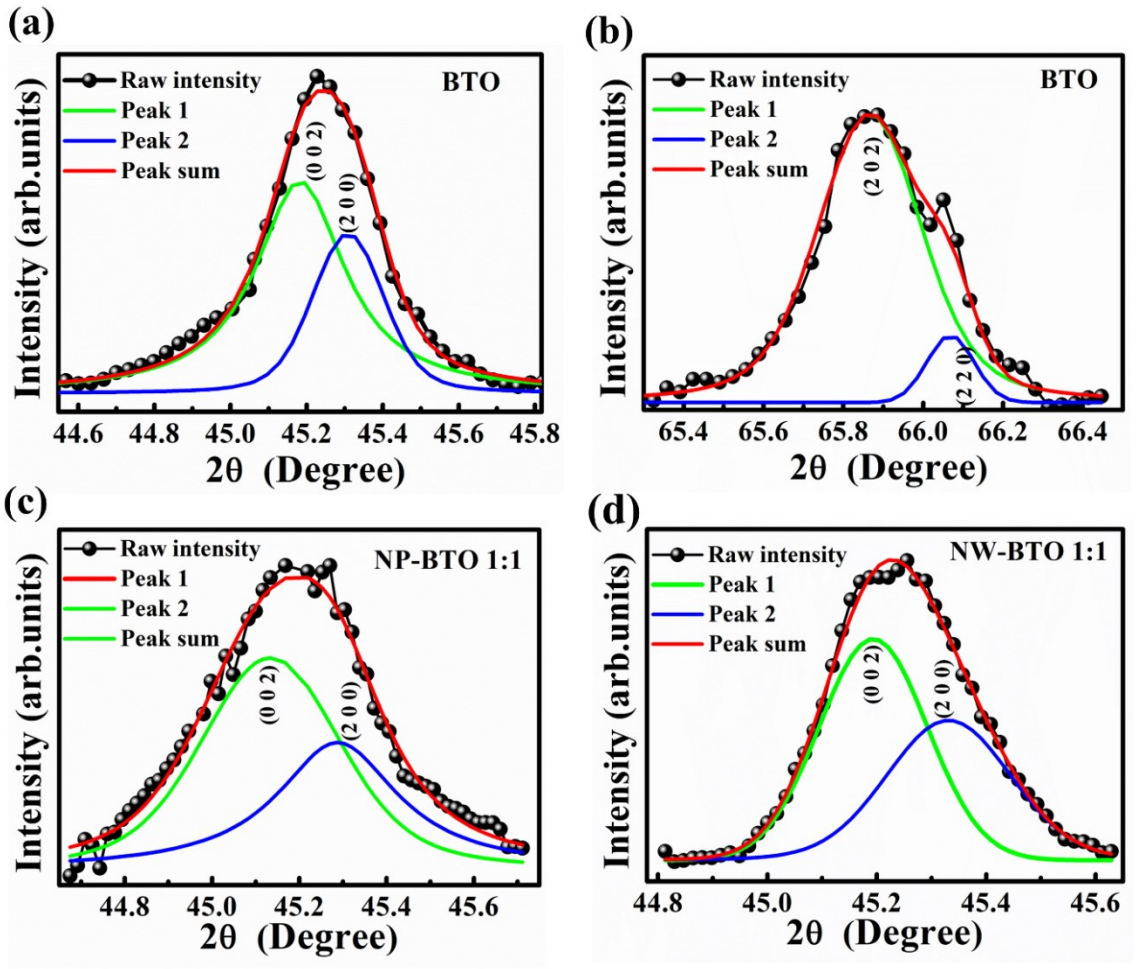
(a)
Raw intensity
Peak 1
Peak 2
Peak sum
BTO
(0 0 2)
(2 0 0)
Intensity (arb.units)
44.6 44.8 45.0 45.2 45.4 45.6 45.8
2θ (Degree)
(b)
Raw intensity
Peak 1
Peak 2
Peak sum
BTO
(2 0 2)
(2 2 0)
Intensity (arb.units)
65.4 65.6 65.8 66.0 66.2 66.4
2θ (Degree)
(c)
Raw intensity
Peak 1
Peak 2
Peak sum
NP-BTO 1:1
(0 0 2)
(2 0 0)
Intensity (arb.units)
44.8 45.0 45.2 45.4 45.6
2θ (Degree)
(d)
Raw intensity
Peak 1
Peak 2
Peak sum
NW-BTO 1:1
(0 0 2)
(2 0 0)
Intensity (arb.units)
44.8 45.0 45.2 45.4 45.6
2θ (Degree)

Fig. S1

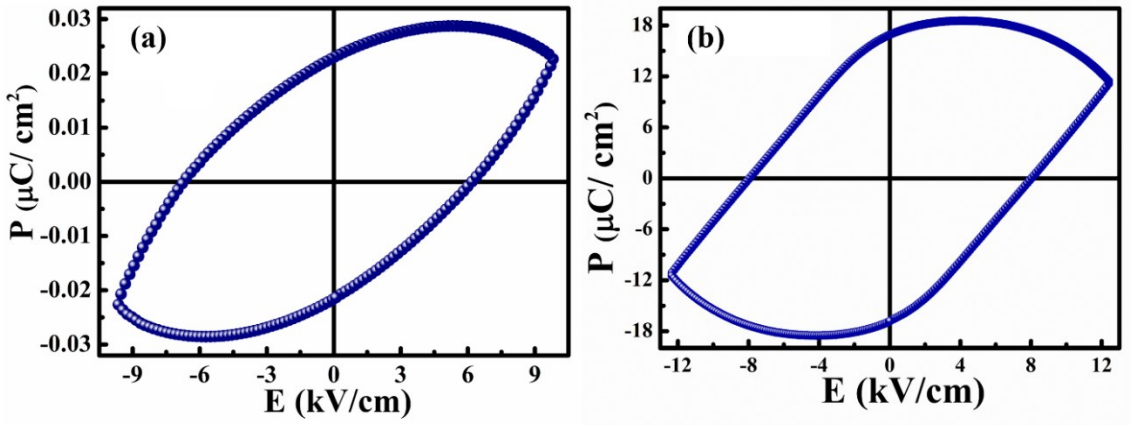
(a)
P (μC/ cm²)
0.03 0.02 0.01 0.00 -0.01 -0.02 -0.03
-9 -6 -3 0 3 6 9
E (kV/cm)
(b)
P (μC/ cm²)
18 12 6 0 -6 -12 -18
-12 -8 -4 0 4 8 12
E (kV/cm)

Fig. S2

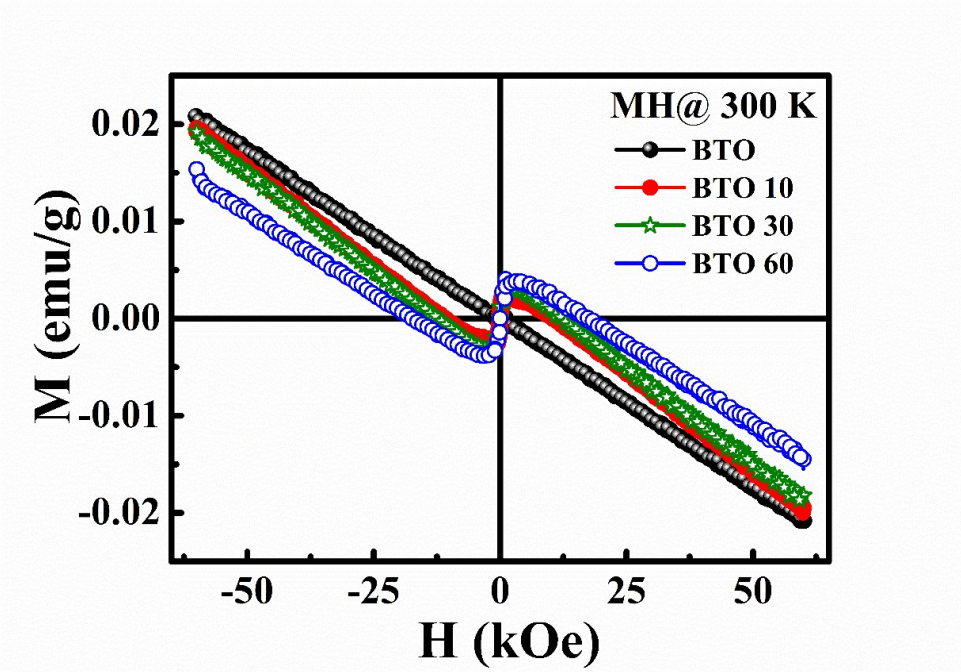
MH@ 300 K
BTO
BTO 10
BTO 30
BTO 60
M (emu/g)
0.02
0.01
0.00
-0.01
-0.02
-50
-25
0
25
50
H (kOe)

Fig. S3

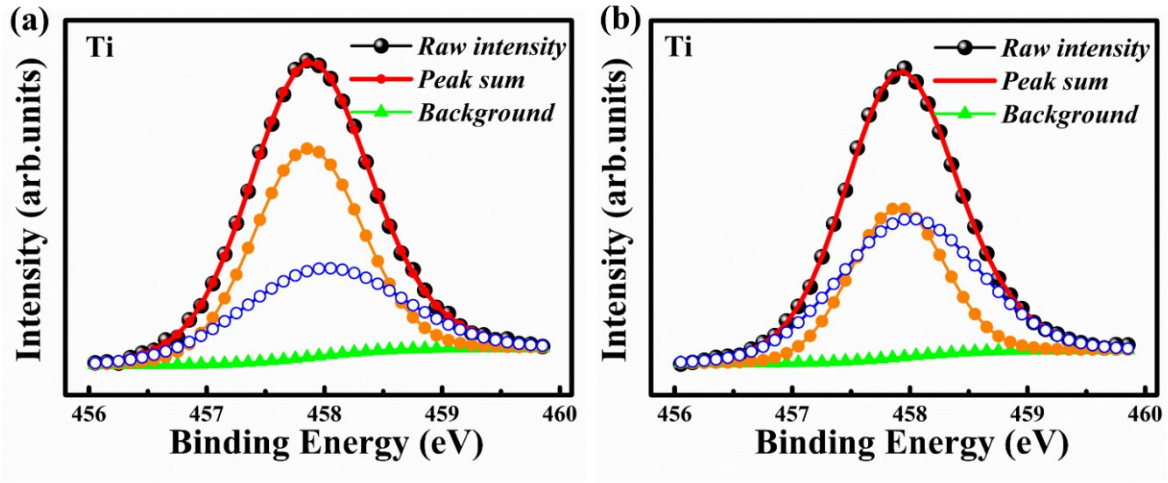
(a)
Ti
Raw intensity
Peak sum
Background
Intensity (arb.units)
456
457
458
459
460
Binding Energy (eV)
(b)
Ti
Raw intensity
Peak sum
Background
Intensity (arb.units)
456
457
458
459
460
Binding Energy (eV)

Fig. S4

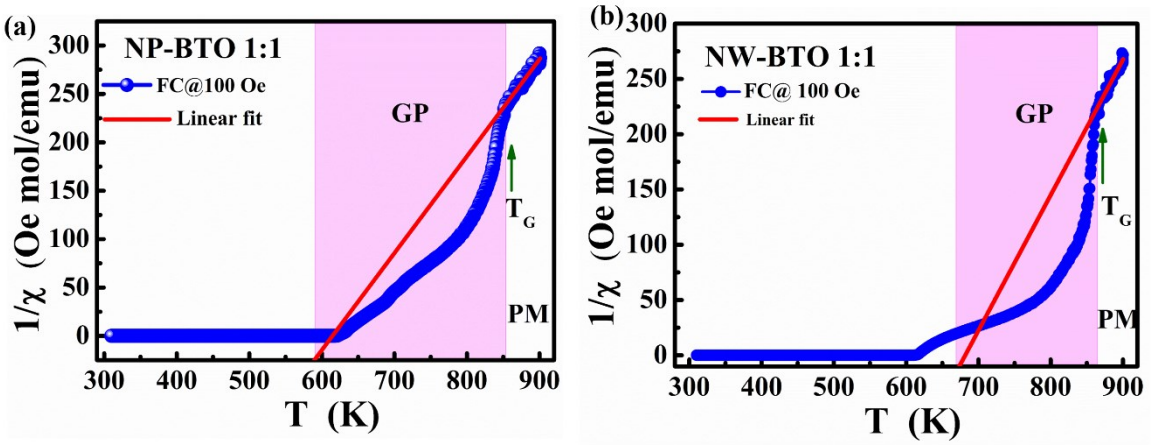
(a)
NP-BTO 1:1
FC@100 Oe
Linear fit
GP
PM
T_G
1/χ (Oe mol/emu)
T (K)
(b)
NW-BTO 1:1
FC@ 100 Oe
Linear fit
GP
PM
T_G
1/χ (Oe mol/emu)
T (K)

Fig. S5

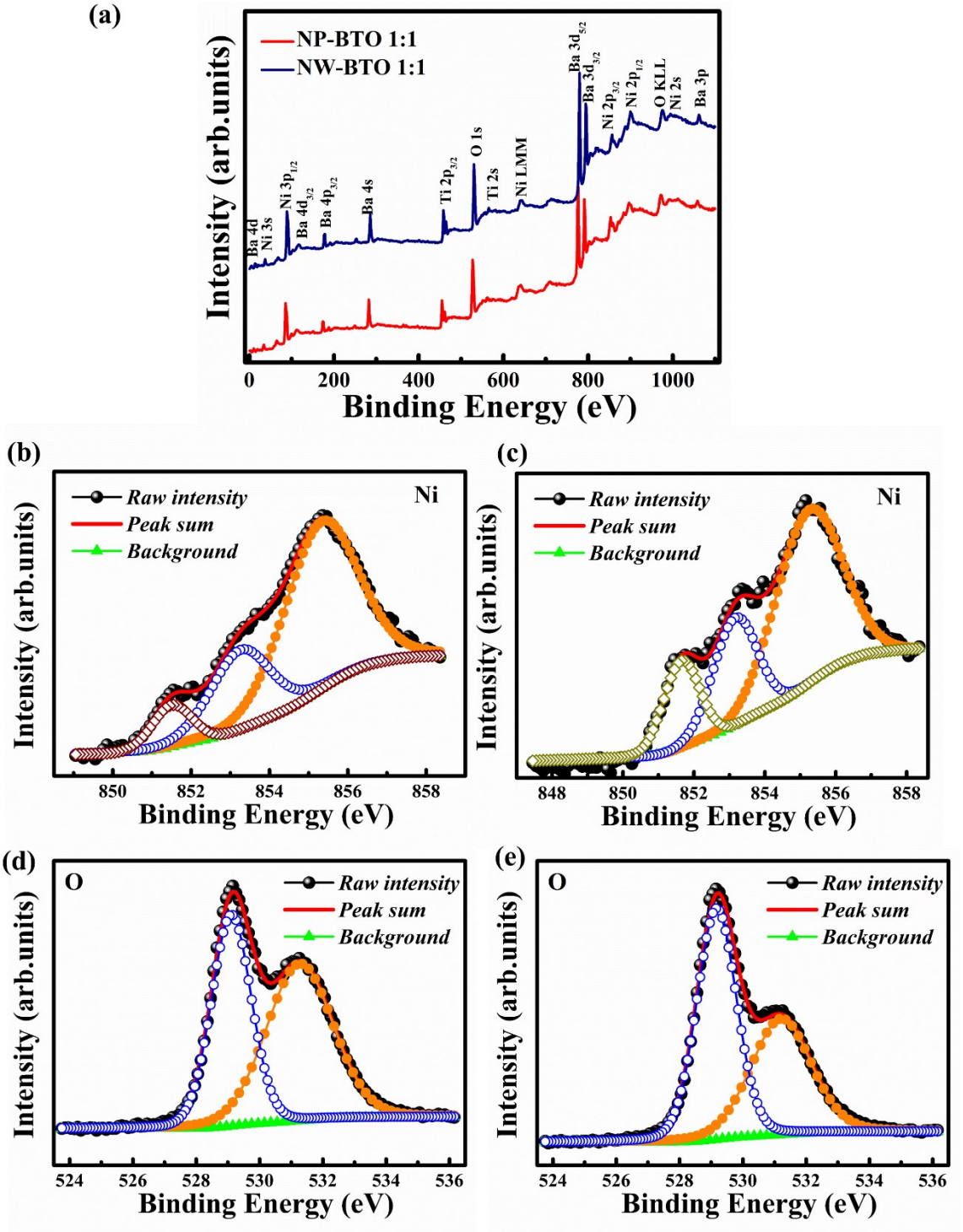
(a)
NP-BTO 1:1
NW-BTO 1:1
Intensity (arb.units)
Binding Energy (eV)
Ba 4d
Ni 3s
Ni 3p1/2
Ba 4d3/2
Ba 4p3/2
Ba 4s
Ti 2p3/2
O 1s
Ti 2s
Ni LMM
Ba 3d5/2
Ba 3d3/2
Ni 2p3/2
Ni 2p1/2
O KLL
Ni 2s
Ba 3p
(b)
Raw intensity
Peak sum
Background
Ni
(c)
(d)
O
(e)

Fig. S6

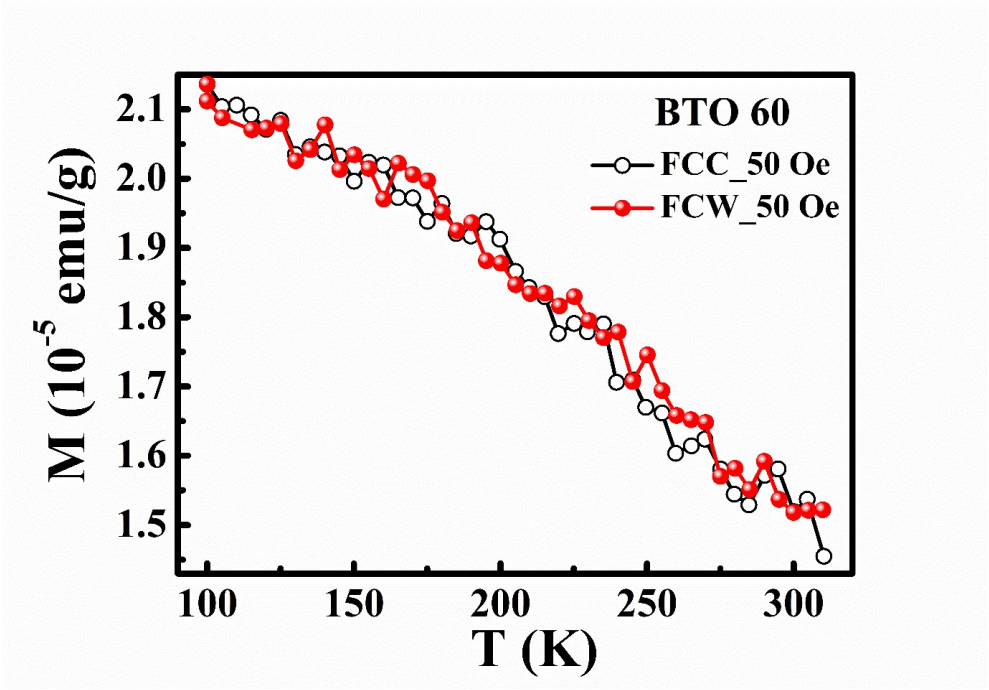
BTO 60
FCC_50 Oe
FCW_50 Oe
M (10^{-5} emu/g)
T (K)
2.1
2.0
1.9
1.8
1.7
1.6
1.5
100
150
200
250
300

Fig. S7

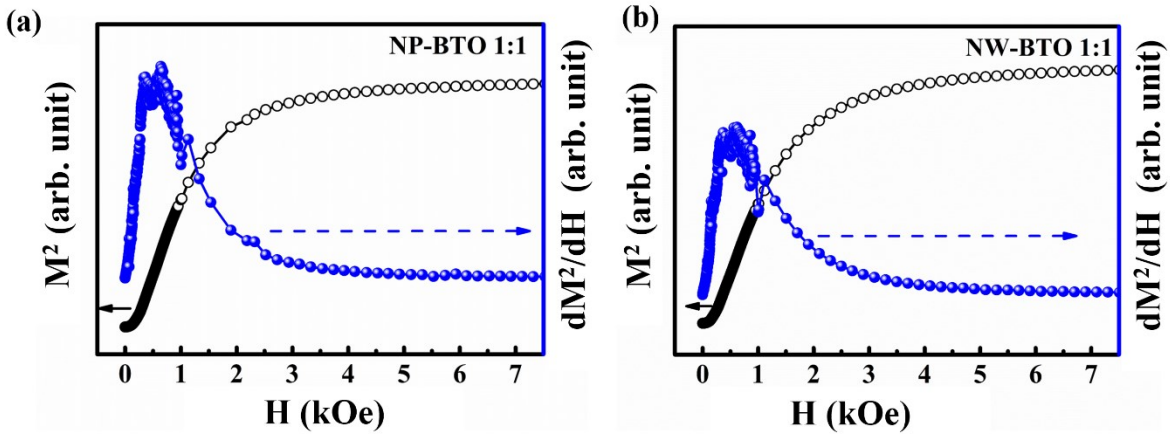
(a)
NP-BTO 1:1
M² (arb. unit)
dM²/dH (arb. unit)
H (kOe)
(b)
NW-BTO 1:1
M² (arb. unit)
dM²/dH (arb. unit)
H (kOe)

Fig. S8

Table. S1. Comparison of ME coefficient of Ni/BTO systems.

Magnetoelectric Ni/BTO system	**Max. α_{ME} (mV/cm.Oe)**	**Reference**
$BaTiO_3$-Ni composite film	----	[1]
Ni-$BaTiO_3$ nanocomposite	----	[2]
$BaTiO_3$-Ni nanocomposite	----	[3]
Ni-$BaTiO_3$ superlattices	----	[4]
$BaTiO_3$-Ni thick film	0.007	[5]
$BaTiO_3$ thin films deposited on polycrystalline Ni foils	90	[6]
$BaTiO_3$ nanotube surrounded by electrodeposited Ni matrix	95	[7]
Ni_x - $(BaTiO_3)_{1-x}$ composites	4.8	[8]
Ni nanowire decorated with BTO nanoparticles	0.517	[9]
NP-BTO 1:1	18.5	This work
NP-BTO 1:2	14.5	This work
NP-BTO 1:5	0.08	This work
NW-BTO 1:1	0.07	This work
NW-BTO 1:2	9.51	This work
NW-BTO 1:5	10.91	This work

Reference in Table.S1

[1] L. Qiao, X. Bi, Evaluation of magnetoelectric coupling in a BaTiO3-Ni composite ferroic film by impedance spectroscopy, Appl. Phys. Lett. 92 (2008) 214101-1–3.

[2] L. Lutsev, S. Yakovlev, V. Castel, C. Brosseau, Spin wave dynamics in magnetoelectric Ni/BaTiO3 nanocomposites, J. Phys. D Appl. Phys. 43 (2010) 325302 1–6.

[3] C. Brosseau, V. Castel, Extrinsic Magnetoelectricity in Barium Titanate-Nickel Nanocomposites : Effect of Compaction Pressure on Interfacial Anisotropy, Spectrosc. Lett. 45 (2012) 471–476.

[4] J.Q. Dai, H. Zhang, Y.M. Song, Interfacial electronic structure and magnetoelectric effect in M/BaTiO3 (M=Ni , Fe) superlattices, J. Magn. Magn. Mater. 324 (2012) 3937–3943.

[5] L.B. Hao, Q.Y. Fu, D.X. Zhou, W. Luo, F. Xue, L. Zhou, Electrical and magnetic properties of bilayered BaTiO3 – Ni thick films prepared via a combined method of electrophoretic deposition and screen printing, J. Mater. Sci: Mater Electron. 24 (2013) 3885–3890.

[6] W. Liang, Z. Li, Z. Bi, T. Nan, H. Du, C. Nan, C. Chen, Q. Jia, Y. Lin, Role of the interface on the magnetoelectric properties of BaTiO3 thin films deposited on polycrystalline Ni foils, J Mater. Chem. C. 2 (2014) 708–714.

[7] S. Siva Vadla, T. Costanzo, S. John, G. Caruntu, S.C. Roy, Local probing of magnetoelectric coupling in BaTiO3 -Ni 1 – 3 composites, Scr. Mater. 159 (2019) 33–36.

[8] T. Buttlar, T. Walther, K. Dörr, S.G. Ebbinghaus, Preparation and Magnetoelectric Behavior of Ni / BaTiO 3 Heterostructures with 0-3 Connectivity, Phys. Stat. Sol (B). 1900622 (2020) 1–8.

[9] R. Revathy, A. Kaipamangalath, M. Raama Varma, K.P. Surendran, BaTiO3 nanoparticle-decorated hierarchical Ni nanowire assemblies for magnetoelectric applications, New J. Chem. 44 (2020) 3690–3699.

Absolute field error correction

In the present manuscript, all the magnetic characterizations were carried out using a physical property measurement system (PPMS-DynaCool, QD, USA) equipped with a 9 Tesla (T) magnet. The origin of the remanent field and methods for its mitigation are outlined in the website of QD (see the QD Application Note 1070-207, Using PPMS superconducting magnets at low fields, https://www.qdusa.com/siteDocs/appNotes/1070-207.pdf, as viewed on 15th May 2021). It is possible to characterize these remnant fields using a standard paramagnetic test sample (see the QD Application Note 1500-021, Correcting for the absolute field error using the Pd standard, https://www.qdusa.com/siteDocs/appNotes/1500-021.pdf, as viewed on 15th May 2021). For mitigating the magnetic field artifacts in measurements, the authors have carried out the M(T) and M(H) measurements of the standard paramagnetic test sample, Palladium (Pd), to directly calculate the susceptibility and true magnetic field. This procedure is invariably conducted during every restart of the PPMS system after the shutdown.

Fig. R1 shows the M(T) measurements of Pd at ±1T field in zero field cooled (ZFC) and field cooled (FC) modes within a temperature range of 290 K to 302 K. From the figure, it is clear that ZFC and FC data at ±1T field produces almost same magnetization values for paramagnetic Pd sample. The obtained χ at 298 K is ~ 5.30×10^{-6} emu/g. Oe. Figs. R2(a) and (b) depict the M(H) data of Pd taken at 298 K and its zoomed-in portion, respectively. From Fig. R2(b), it is clear that at low fields, the moment is hysteretic. At zero reported field, the moment is not zero as would be expected for a perfect paramagnet. Here, a remanent field of ~ 20.33 Oe is obtained in the (-H) axis. From the M(H) data, we can calculate the true field of the Pd standard using the equation, True field = $\frac{M}{\chi \text{ at } 298 \text{ K}}$, where moment (M) is in emu/g.

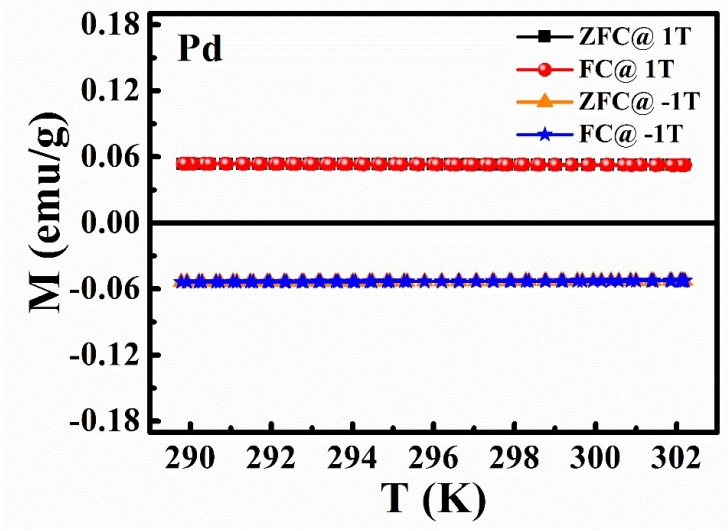

Fig. R1: M(T) measurements taken at a field of ±1T

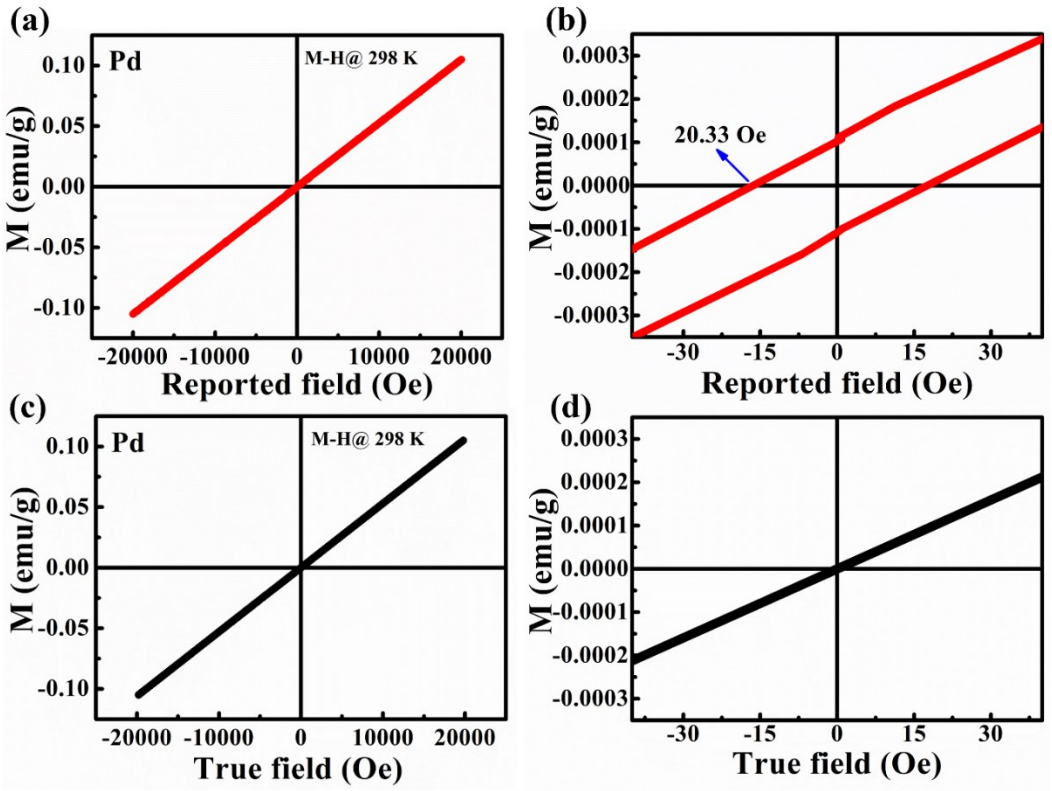

Fig. R2: M(H) measurements at 298 K for standard paramagnetic Pd sample

In Fig. R2(c), M is plotted as a function of the calculated true field, and its zoomed-in portion is shown in Fig. R2(d). Then, there is no hysteresis formation in the M(H) data (see Fig.R2(d)). Hence the remanent field is avoided by considering the true field of the sample. So, correcting the absolute field error using the Pd standard is an excellent option to mitigate the remanent field.

Since the remanent properties of the magnet are reproducible, we can apply the obtained field correction of ~20.33 Oe to our measured sample of interest. For that, magnetic field oscillations were carried out between +1 T and -1 T. Then, slowly reduces the 1 T field with a step size of 50 Oe and, finally brought to the field that can cancel out the remanent field. So, we modified the magnetic field set points of the program sequence file as +20.33 Oe from positive high fields so that the actual measured field is the true field, and that will produce a remanent field of ~0 Oe (see the QD Application Note 1070-207, mentioned above). For assuring the zero remanent field, we had measured all the samples using the above-mentioned protocol. Hence, in the present study, the room temperature coercivities obtained for the samples NP and NW are not in the error range of VSM. The slight increment in coercivity of soft ferromagnetic Ni from 120 Oe to 140 Oe is attributed to the morphology change from zero-dimensional NP to one dimensional NW due to the shape anisotropy of one dimensional Ni nanowires.